JOURNAL OF GEOPHYSICAL RESEARCH: SPACE PHYSICS, VOL. 118, 299–312, doi:10.1029/2012JA018349, 2013

# The role of transient ion foreshock phenomena in driving Pc5 ULF wave activity

M. D. Hartinger,[1,2] D. L. Turner,[2] F. Plaschke,[2] V. Angelopoulos,[2] and H. Singer[3]

Received 17 July 2012; revised 11 November 2012; accepted 13 November 2012; published 31 January 2013.

[1] The ion foreshock is a source of energy for magnetospheric ULF waves, but it is usually only considered effective at driving ULF waves with frequencies above the Pc5 (2–7 mHz) range. We present observations for an 8 h high speed solar wind interval on 14 July 2008 during which three distinct types of transient ion foreshock phenomena (TIFP) were observed just upstream of the dayside bow shock. We demonstrate that TIFP generate global magnetospheric Pc5 ULF waves with amplitudes as large as 10 mV/m in the electric field and 10 nT in the magnetic field. We characterize the magnetospheric ULF response to several different TIFP that occur during this interval, including the first report of the ULF response to a foreshock bubble. Using a novel spacecraft configuration, we find that the local time with the highest Pc5 wave amplitude is closely related to the location of the ion foreshock. Statistical studies of Pc5 ULF wave activity, other case studies of ULF waves driven by processes in the ion foreshock, and recent theoretical and simulation work on TIFP place these results in context: TIFP are an important energy source for Pc5 ULF waves in the magnetosphere.

**Citation:** Hartinger, M. D., D. L. Turner, F. Plaschke, V. Angelopoulos, and H. Singer (2013), The role of transient ion foreshock phenomena in driving Pc5 ULF wave activity, *J. Geophys. Res. Space Physics*, *118*, 299–312, doi:10.1029/2012JA018349.

## 1. Introduction

[2] The ion foreshock is a region in the solar wind magnetically connected to the Earth's bow shock. It contains ions with a range of energies that are distinct from the bulk solar wind flow. While streaming against the solar wind flow, these ions generate a number of instabilities that can lead to perturbations in the ion foreshock; these perturbations can ultimately affect the Earth's magnetosphere [*Eastwood et al.*, 2005].

[3] The ion foreshock is an important energy source for Ultra Low Frequency waves in the Earth's magnetosphere, although it is usually associated with wave frequencies above the Pc5 range (2–7 mHz) [e.g., *Troitskaya et al.*, 1971; *Russell and Hoppe*, 1983; *Chi et al.*, 1994; *Eastwood et al.*, 2011]. Studies of ion foreshock ULF waves established that both the frequency of the waves in the ion foreshock and the frequency of the waves in the magnetosphere are strongly correlated with the magnitude of the interplanetary magnetic field (IMF); this suggests that they are generated in the ion foreshock via a cyclotron instability [*Troitskaya et al.*, 1971]. They also occur primarily in the Pc3-4 frequency range (7 to 100 mHz, [*Jacobs et al.*, 1964]) and in the dayside magnetosphere. They are observed in the magnetosphere during intervals when the IMF cone angle is low. The cone angle is defined as

$$\arccos\frac{B_x}{|B|} \tag{1}$$

where $|B|$ is the total IMF and $B_x$ is the GSM/GSE $x$ component of the IMF. When the cone angle is low, the ion foreshock is located near the subsolar dayside magnetosphere; it is then more effective at driving magnetospheric ULF waves [*Chi et al.*, 1994].

[4] The ion foreshock is not typically considered an important energy source for ULF waves in the Pc5 frequency range. The main reason is the high degree of correlation often found between magnetospheric Pc5 wave power and geomagnetic activity indices or pristine solar wind conditions, with a comparatively low degree of correlation with IMF cone angle. For example, *Takahashi and Ukhorskiy* [2007] found that pristine solar wind (i.e., not ion foreshock) dynamic pressure variations were strongly correlated with Pc5 wave power measured at geosynchronous orbit near the noon local time sector, and *Liu et al.* [2010] found strong correlations with solar wind flow speed in the flank magnetosphere. *Sanny et al.* [2007] found that the IMF cone angle did not correlate significantly with compressional Pc5 wave power at geosynchronous orbit when compared with pristine solar wind pressure and flow speed correlations. The statistical results from these studies casts doubt on the importance

[1]Department of Atmospheric, Oceanic, and Space Sciences, University of Michigan, Ann Arbor, Michigan, USA.
[2]Department of Earth and Space Sciences, UCLA, Los Angeles, California, USA.
[3]NOAA Space Weather Prediction Center, Boulder, Colorado, USA.

Corresponding author: M. D. Hartinger, Space Research Building, University of Michigan, 2455 Hayward St., Ann Arbor, MI 48109-2143, USA. (mdhartin@umich.edu)


2169-9380/13/2012JA018349

(relative to other energy sources) of the ion foreshock as a driver of Pc5 ULF wave activity.

[5] There is some evidence suggesting that the ion foreshock could play a role in driving Pc5 waves. *Miura* [1992] proposed that the ion foreshock may seed surface waves at locations where the magnetopause is Kelvin-Helmholtz unstable. This could explain a pronounced dawn-dusk asymmetry, which is often observed in statistical studies of Pc5 ULF wave activity, particularly in studies using ground observations [e.g., *Yumoto et al*., 1983; *Chisham and Orr*, 1997]. Based on the classic picture of the Parker spiral in the solar wind, the ion foreshock is nominally located in the dawn/prenoon sector, where a statistical peak in Pc5 ULF wave power is often observed. If the dawn flank is unstable to the growth of magnetopause surface waves via the Kelvin-Helmholtz instability (KHI), pulsations originating in the ion foreshock could provide a seed for surface wave growth; these surface waves would ultimately drive Pc5 wave activity in the magnetosphere.

[6] *Nosé et al*. [1995] conducted a test to determine whether the ion foreshock plays an important role in seeding the KHI. Using Dynamics Explorer 1, a polar orbiting spacecraft, they identified periods of enhanced transverse Pc5 wave activity while recording the conditions in the solar wind. Using a model for the bow shock, they then determined whether the quasi-parallel bow shock (ion foreshock) was located in the same magnetic local time sector as the observation, finding that this was the case for a variety of solar wind conditions (see Figure 5 in that paper). Their results show that the ion foreshock plays a role in determining the dawn-dusk asymmetry often observed in statistical studies of Pc5 wave power. They proposed that the ion foreshock provided seed fluctuations for the growth of magnetopause surface waves, consistent with *Miura* [1992]. *Sanny et al*. [2002] also found that statistically significant peaks in Pc5 wave power were colocated with the expected location of the quasi-parallel bow shock for both spiral ($\vec{B}_x \cdot \vec{B}_y < 0$) and orthospiral ($\vec{B}_x \cdot \vec{B}_y > 0$) IMF orientation. Finally, *Sanny et al*. [2007] found a prenoon peak in compressional Pc5 wave power during intervals of low geomagnetic activity that was likely associated with the ion foreshock.

[7] Transient phenomena occurring within the ion foreshock are a potential source of energy for magnetospheric ULF waves [e.g., *Russell and Hoppe*, 1983; *Eastwood et al*., 2011]. We here define the transient ion foreshock phenomena (TIFP) as an umbrella term that encompasses a variety of phenomena, some of which may have overlapping definitions [*Eastwood et al*., 2005]. They can be differentiated from ion foreshock ULF waves because of their transient nature; unlike ULF waves in the ion foreshock, which have been observed to be steady with enhancements at nearly the same frequency for many wave cycles, TIFP are not monochromatic waves.

[8] Recently, hybrid kinetic models and multispacecraft observations have led to more detailed descriptions of some TIFP, including foreshock cavities [e.g., *Sibeck et al*., 2002], hot flow anomalies (HFAs) [e.g., *Thomas and Brecht*, 1988; *Paschmann et al*., 1988; *Eastwood et al*., 2011], bow shock ripples [e.g., *Hietala et al*., 2009], and foreshock bubbles (FB) [*Omidi et al*., 2010]. These phenomena may have very different properties, but we shall group them together for the purpose of differentiating them from other potential energy sources of ULF waves in the magnetosphere; namely, ULF waves in the ion foreshock, dynamic pressure fluctuations in the pristine solar wind, flow shear instabilities on the magnetopause, dayside reconnection, and wave particle interactions. All TIFP share one characteristic important for the present study: they can lead to variations in the upstream dynamic, thermal, and/or magnetic pressure, which can excite ULF waves in the magnetosphere in much the same manner as dynamic pressure pulses in the pristine solar wind. Thus, they are not band-limited to the Pc3-4 frequency range [*Fairfield et al*., 1990; *Southwood and Kivelson*, 1990; *Eastwood et al*., 2011].

[9] A few studies have established that TIFP can generate ULF waves in the Earth's magnetosphere. *Fairfield et al*. [1990] presented evidence that pressure pulses originating in the ion foreshock could excite ULF perturbations in the magnetosphere at frequencies in the Pc5 range. *Sanny et al*. [1996] showed that transient bipolar magnetic field signatures observed in the Earth's magnetosphere are likely related to pressure pulses in the pristine solar wind or ion foreshock rather than dayside reconnection events. *Sanny et al*. [2001] further showed that these bipolar signatures were observed in locations consistent with excitation by ion foreshock processes; these signatures were also preceded by IMF discontinuities, consistent with the formation mechanisms of many TIFP [e.g., *Omidi and Sibeck*, 2007; *Omidi et al*., 2010]. *Eastwood et al*. [2011] showed that an HFA originating in the ion foreshock excited standing Alfvén waves with Pc3 frequency in the Earth's magnetosphere. *Hietala et al*. [2012] showed that supermagnetosonic jets originating from the quasi-parallel bow shock had several magnetospheric impacts, including the excitation of ULF waves at geosynchronous orbit. Ground magnetometer observations near the cusp and polar cap provide additional suggestive evidence that TIFP may generate ULF waves in the magnetosphere. *Kataoka et al*. [2003] and *Murr and Hughes* [2003] found that magnetic impulse events and traveling convection vortices tend to occur in conjunction with TIFP; both phenomena can have Pc5 periods and both can be associated with magnetospheric ULF wave activity [*Shields et al*., 2003].

[10] In two studies, we shall examine the response of the magnetosphere to TIFP during an interval of high speed solar wind that occurred on 14 July 2008. In this study, we focus entirely on the ULF response of the magnetosphere to TIFP, whereas Turner et al. (manuscript in preparation, 2012c) will be focused on global responses of the magnetosheath/magnetosphere/ionosphere system to TIFP. We demonstrate here that TIFP generate Pc5 wave activity with large amplitudes (10 nT, 10 mV/m) comparable to storm time ULF waves [*Walker et al*., 1982]. A unique spacecraft configuration enables us to show for the first time that a variety of different TIFP can drive Pc5 ULF waves with different properties. This configuration also reveals that the location with peak wave amplitude at geosynchronous orbit can vary rapidly as the ion foreshock morphology changes; this is the first direct observation of this relationship (made possible through continual monitoring of geosynchronous orbit in the dawn, noon, and

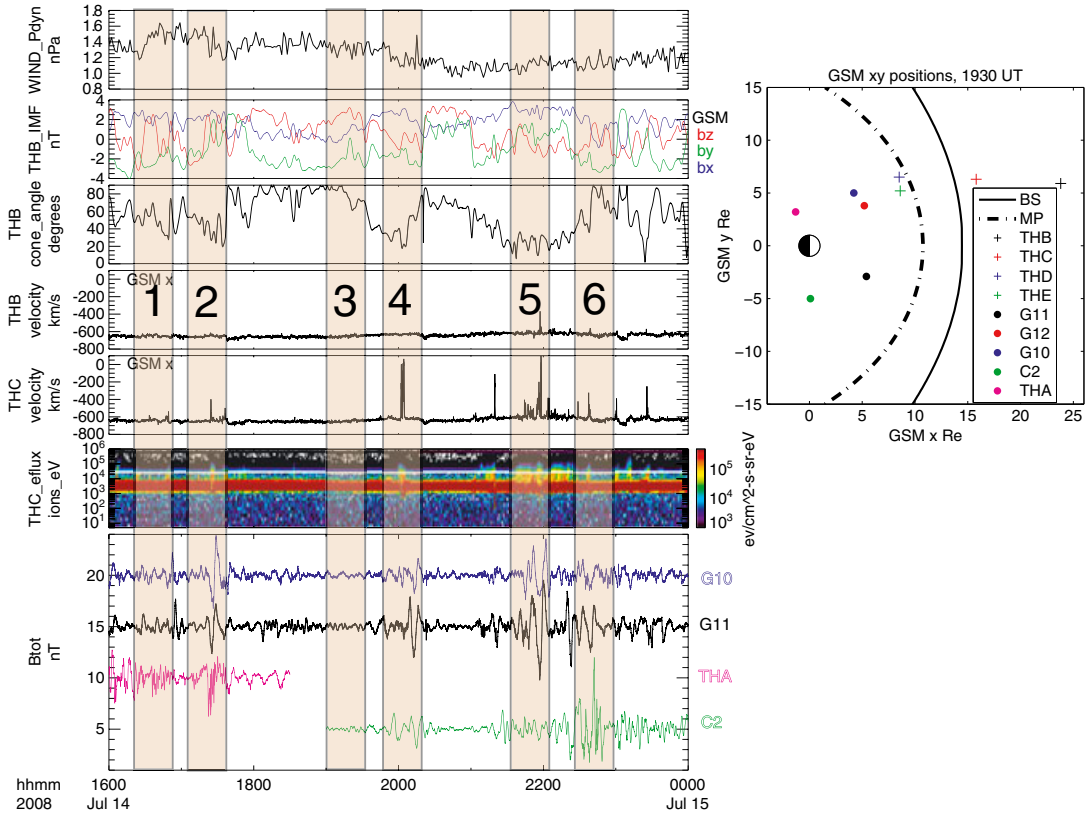


**Figure 1.** An overview showing the relationship between TIFP and ULF wave observations in the magnetosphere. From top to bottom: (1) the solar wind dynamic pressure from OMNIweb, (2) the IMF from THB, (3) IMF cone angle from THB, (4) the GSM x component of the velocity measured at THB, (5) the same for THC, (6) the ion energy flux spectrogram from THC, and (7) the total magnetic field perturbation measured at G10, G11, THA, and C2. Numbered tan boxes indicate shorter intervals of interest in Figure 2. The inset is for the spacecraft positions in the GSM *xy* plane.

dusk local time sectors over an eight hour period), bolstering previous statistical evidence. In situ monitoring of the ion foreshock reveals that the TIFP generate significant dynamic pressure fluctuations. We propose that these fluctuations alone can explain the large amplitude magnetospheric ULF waves. In contrast to the mechanism proposed by *Miura* [1992] and *Nosé et al*. [1995], our observations suggest that a KH-unstable magnetopause is not required for the ion foreshock to generate significant Pc5 wave activity. Finally, simultaneous observations of the IMF cone angle and Pc5 response of the magnetosphere show that correlations (or lack thereof) between the cone angle and magnetospheric Pc5 wave activity are sensitive to the time chosen to compute the cone angle. We propose that this sensitivity may provide an explanation for the low degree of correlation often found between IMF cone angle and magnetospheric Pc5 wave activity [e.g., *Chi et al*., 1994; *Sanny et al*., 2007], arguing in favor of the ion foreshock playing a more important role in driving Pc5 wave activity than previously thought.

## 2. Instrumentation

[11] We use data from the five-satellite Time History of Events and Macroscale Interactions During Substorms (THEMIS) mission [*Angelopoulos and Sibeck*, 2008; *Sibeck and Angelopoulos*, 2008]. Each spinning satellite (3 s spin period) is equipped with a fluxgate magnetometer (FGM) [*Auster et al*., 2008], an electric field instrument [*Bonnell et al*., 2008], an ion and electron electrostatic analyzer (ESA) [*McFadden et al*., 2008], and ion and electron solid state telescopes (SST) [e.g., *Turner et al*., 2012a]. ESA measures the three-dimensional particle distributions and moments (electrons: 5 eV to 30 keV, ions 5 eV to 25 keV) once per spin. SST also measures the three-dimensional particle distributions and moments once per spin and is sensitive to energies above 25 keV. Electric field instrument measures ULF perturbations best for the two components in the spacecraft spin plane; we use these two components, the magnetic field measured by FGM, and the $E * B = 0$ approximation to obtain the third component of the electric field.

[12] We also use data from the Geostationary Operational Environmental Satellites (GOES) and Cluster spacecraft. Specifically, we use data from GOES-10, GOES-11, GOES-12, and Cluster-2. GOES and Cluster are equipped with fluxgate magnetometers [*Singer et al*., 1996; *Balogh et al*., 2001]. Finally, we obtained hourly geomagnetic activity indices and both hourly and minute resolution solar wind data from the Space Physics Data Facility (a project of

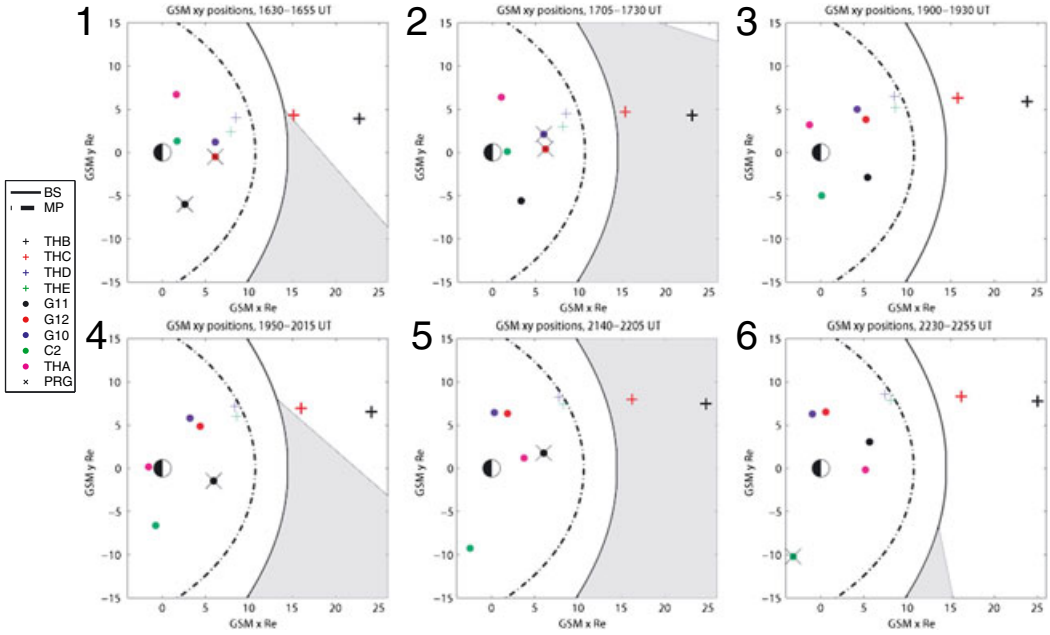


**Figure 2.** These plots show the connection between the ion foreshock location and the location where peak ULF wave amplitude is observed in the magnetosphere near geosynchronous orbit. Numbered panels correspond to intervals of interest from Figure 1. Each panel shows the probe positions and ion foreshock location in the GSM *xy* plane during the interval; the solid black line indicates the bow shock and the dot-dashed line indicates the magnetopause. The *x*'s indicate the location of the peak ULF wave response measured at geosynchronous orbit (referred to as PRG in the legend)—panel three does not have an *x* because no significant ULF wave activity occurred during that interval.

NASA's Goddard Space Flight Center) OMNIWeb interface at http://omniweb.gsfc.nasa.gov.

## 3. Observations and Analysis

### 3.1. Event Overview

[13] We studied the ULF response of the magnetosphere to TIFP during the interval from 1600 to 2400 UT on 14 July 2008. This interval is a subset of a larger interval, 14 July 2008 1200 UT to 15 July 2008 1200 UT, described in a second study examining more fully the response of the magnetosphere and ionosphere to TIFP (i.e., Turner et al., manuscript in preparation, 2012c). We chose this particular subset because probe positions in the dayside magnetosphere were ideal for observing ULF wave variation as a function of magnetic local time. The event occurred during the passage of a high speed stream, as the solar wind flow speed was approximately 650 km/s, significantly higher than nominal conditions of about 400 km/s [*Hapgood et al.*, 1991]. Geomagnetic activity was low ($Kp \leq 3$, $Dst \sim 15$).

[14] Figure 1 shows spacecraft observations in the pristine solar wind, ion foreshock, and magnetosphere during the interval of interest. The top panel is for the pristine solar wind dynamic pressure obtained from the OMNIweb; these data have been propagated to the Earth's bow shock. The dynamic pressure is about 1.2–1.6 nPa with fluctuations of the order 0.1–0.2 nPa throughout the eight hour interval; notably, the fluctuation level remains steady and there are no large spikes (i.e., spikes are small when compared with the TIFP pressure pulses described below).

[15] Panels two through four are for THEMIS-B (THB), which is mostly located in the pristine solar wind but also in the ion foreshock, about 25 Re upstream of the Earth. We apply an 81 s time shift to all data from THB (here and in other figures) to account for propagation delays to the bow shock. Panels two and three show the IMF and cone angle after application of a 2 min boxcar window to smooth the data (to remove higher frequency fluctuations observed when THB is in the ion foreshock). To more clearly identify periods of radial IMF when the ion foreshock ought to be located near the noon local time sector, we transform all cone angles greater than 90° according to $\theta \rightarrow |180 - \theta|$. There are significant fluctuations in the IMF and although the cone angle is low (<45°, corresponding to radial IMF) for about half of the interval, there are several excursions above 45°. Panel four shows the GSM *x* component of the solar wind flow velocity computed using the electrostatic analyzer and solid state telescope ion instruments. The solar wind flow velocity, mostly in the *x* direction, is about 650 km/s and decreasing during the interval. However, there is a large spike in the *x* component at ~2150 UT. During this period, THB magnetic field observations (see Figure 2 for foreshock location based on magnetic field) and observations of a population of energetic ions distinct from the bulk solar wind flow indicate that THB was in the ion foreshock ([e.g., *Fairfield et al.*, 1990; *Eastwood et al.*, 2005] - particle data are not shown); the large spike in velocity suggests the presence of a TIFP.

[16] Panels five and six are for THEMIS-C (THC); THC is located in either the pristine solar wind or ion foreshock during the interval, but mostly in the ion foreshock, and it is

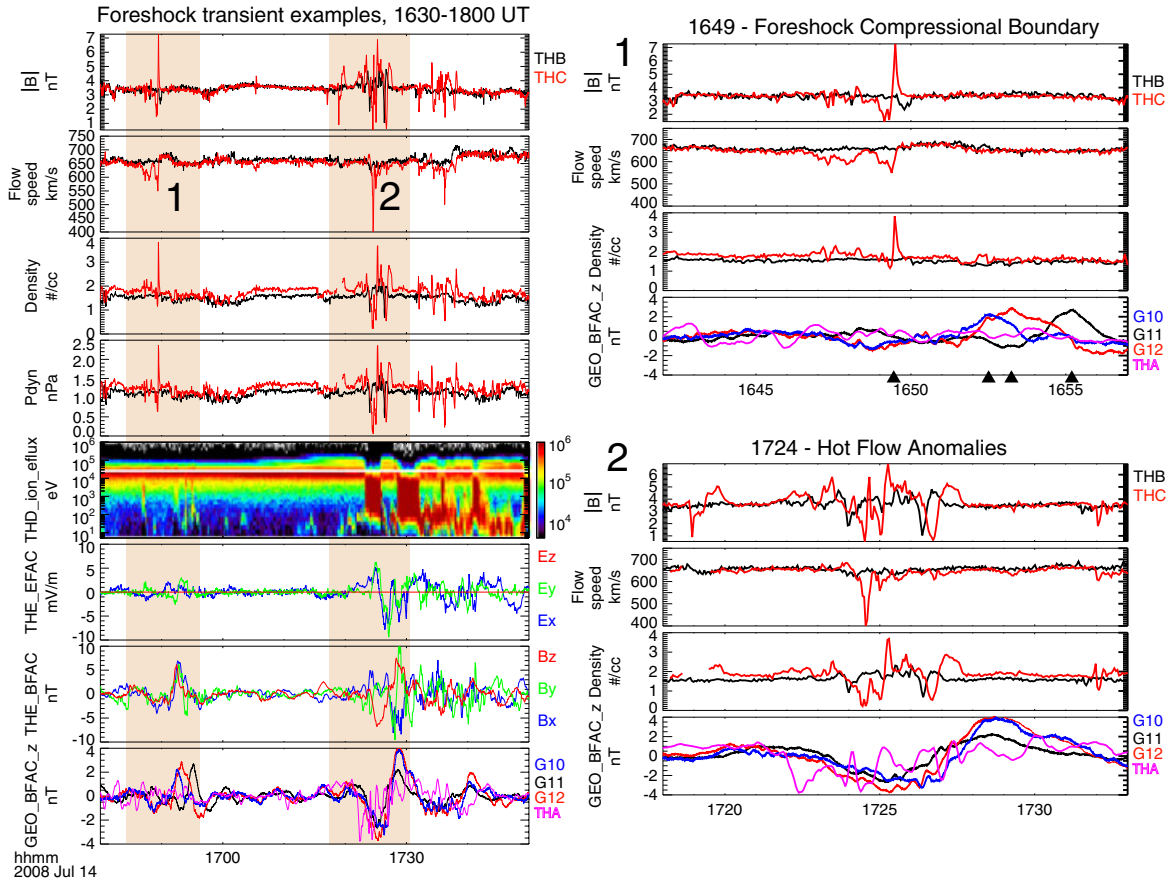


**Figure 3.** These plots show observations in the pristine solar wind, ion foreshock, near the magnetopause, and in the magnetosphere for two TIFP events (foreshock compressional boundary motion and hot flow anomalies). On the left, from top to bottom: (1) total magnetic field; (2) flow speed; (3) density; (4) dynamic pressure observed at THB (black) and THC (red); (5) ion energy flux spectrogram observed at THD; (6) perturbation electric fields observed at THE (field-aligned coordinates, *z* (red) is along the field, *y* (green) points eastward, and *x* (blue) completes the right-hand orthogonal set and is pointed radially outward); (7) perturbation magnetic fields observed at THE; and (8) total magnetic field perturbation observed at G10 (blue), G11 (black), G12 (red), and THA (pink). Numbered tan boxes indicate shorter intervals to plot the same data found in the top three panels and bottom panel in insets on the right.

about 17 Re upstream of the Earth. We apply a 7 s time shift to all data from THC (here and in other figures) to account for propagation delays to the bow shock. Panel five is for the GSM *x* component of the solar wind velocity computed using the ESA and SST ion detectors. The overall trend is consistent with THB, but there are several spikes. Some of the spikes are large enough that the *x* component approaches zero or becomes positive; these changes in the velocity *x* component are caused by TIFP such as HFAs and FBs, as shown in previous simulations and observations [e.g., *Omidi et al.*, 2010]. In this case study, spikes in the velocity *x* component always corresponded to reductions in the flow speed and usually corresponded to flow deflections. Panel six is for an ion energy flux spectrogram that combines data from ESA and SST. The red band of enhanced flux at several keV indicates the bulk flow of the solar wind. Enhancements at energies above this band, such as at 2140–2230 UT, indicate the presence of ion foreshock plasma [e.g., *Fairfield et al.*, 1990]. During periods when THC observed the ion foreshock plasma it was located in the ion foreshock and could detect TIFP; during other periods, TIFP may still occur but they are not detectable by THC because it is not in the ion foreshock.

[17] Panel seven is for observations from GOES-11 (G11, black), GOES-10 (G10, blue), Cluster-2 (C2, green), and THEMIS-A (THA, pink), which are all located in the magnetosphere; they are either in geosynchronous orbit (i.e., GOES) or pass through the radial distance corresponding to geosynchronous orbit during portions of the interval (i.e., THA, C2). The total magnetic field perturbation, obtained by applying a high pass filter (frequency $> 0.5$ mHz; a low pass filter is convolved with the signal in the time domain, and the low pass filtered data are subtracted from the original signal to obtain the high pass filtered data) to the magnetic field magnitude, is shown for each probe. All four probes detect compressional ULF waves during this interval with amplitudes of several nT. The waves that are easily discernible in this panel have periods that are roughly 5 to 10 min ($\sim$2 mHz), although higher frequency waves are also present (shown more clearly in Figure 5). The wave activity is not

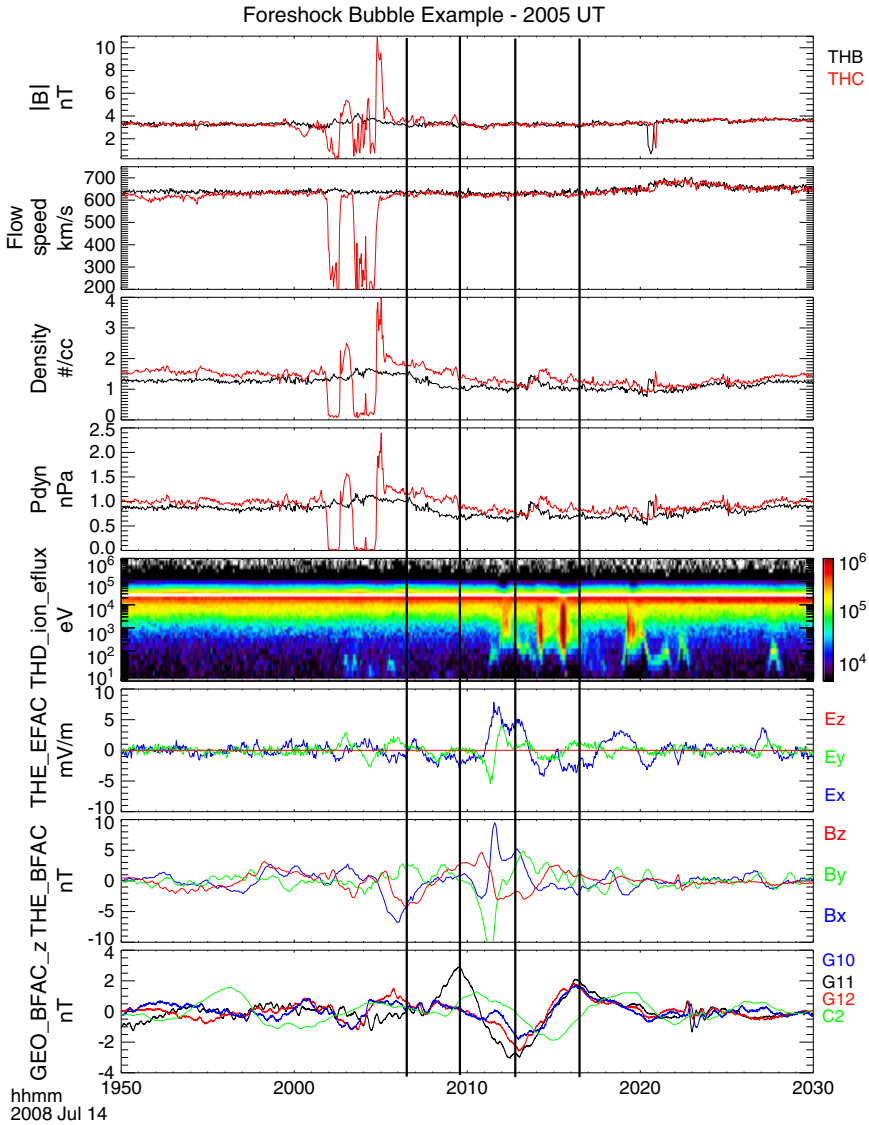


**Figure 4.** This plot shows observations in the pristine solar wind, ion foreshock, near the magnetopause, and in the magnetosphere for one TIFP event (foreshock bubble). From top to bottom: (1) total magnetic field; (2) flow speed; (3) density; (4) dynamic pressure observed at THB (black) and THC (red); (5) ion energy flux spectrogram observed at THD; (6) perturbation electric fields observed at THE (field-aligned coordinates); (7) perturbation magnetic fields observed at THE; and (8) total magnetic field perturbation observed at G10 (blue), G11 (black), G12 (red), and C2 (green). Black lines indicate times for comparing the ULF response at different probes (see text)

steady; enhancements are closely related to TIFP-induced changes in the *x* component of the solar wind velocity observed at THC.

### 3.2. The Relationship Between Ion Foreshock Morphology and ULF Wave Activity

[18] The seventh panel Figure 1 demonstrates that enhancements in ULF wave activity do not occur uniformly in all local time sectors. We further examine this trend in Figure 2. Panels 1 through 6 show the probe positions in the GSM *xy* plane during six intervals of ULF wave activity, marked in yellow in Figure 1. The curved, solid black line indicates the *Fairfield* [1971] bow shock location and the dot-dashed black line indicates the *Shue et al.* [1997] magnetopause location. The gray shaded area in each inset is the approximate location of the ion foreshock; this location changes throughout the interval as the IMF changes. These insets only show the ion foreshock projection in the GSM *xy* plane (the ion foreshock is inherently a three-dimensional structure).

[19] In all the panels of Figure 2, the slanted crosses indicate the location of the peak ULF response at geosynchronous; they are for the largest amplitude perturbation observed at any of the probes during the inset interval. The peak ULF response at geosynchronous is obtained by visually inspecting the total magnetic field perturbation for all probes near geosynchronous orbit (see Figure 1 seventh panel, and Figures 3 and 4). It is meant to indicate differences in wave power due to position in local time rather than radial distance; thus, the responses at THEMIS-D and THEMIS-E (the probes located at larger radial distances) are not considered.

[20] In the first two intervals/panels of Figure 2, THA is close to geosynchronous orbit and is used as a ULF wave monitor in the dusk sector while G10, G11, and G12 are used as monitors at noon and dawn (C2 is near perigee). The first panel shows similar, peak responses near noon and dawn, as indicated by the black crosses at G12 and G11 in the figure, with a weaker response at dusk. The second panel indicates that both the location of the ion foreshock and the peak ULF response at geosynchronous have shifted toward the noon local time sector; G10 and G12 see the largest ULF response to the TIFP.

[21] In the last four intervals/panels of Figure 2, C2 is used as a ULF wave monitor at dawn, G11 at noon, and G10/G12 at dusk (THA is near perigee). During the third interval (panel 3), the ion foreshock is not located upstream from the dayside magnetosphere and conditions are unfavorable for TIFP to affect the magnetosphere. During this period, ULF wave amplitudes are low at all local times, and no peak ULF response at geosynchronous is recorded. During the fourth interval (panel 4), the ion foreshock is located in the noon and dawn sectors and the peak ULF response at geosynchronous is observed prenoon at G11. During the fifth interval (panel 5), the ion foreshock is located throughout the noon local time sector and covers more of the dusk local time sector than in the previous interval. The peak ULF response at geosynchronous is again seen at G11 at noon with a slightly weaker response at G10/G12 at dusk and weakest response at dawn at C2; the amplitude at C2 may also be lower due to its larger distance from the magnetopause than the other two probes. Finally, during the sixth interval (panel 6), the ion foreshock is located in the dawn sector and C2 sees the peak ULF response at geosynchronous despite being further from the magnetopause than G11 and G10. G11 sees the next largest response and G10/G12 sees the weakest response, consistent with their relative distances from the dawn local time sector/ion foreshock location.

### 3.3. Isolated TIFP Examples: Foreshock Compressional Boundary Motion and Hot Flow Anomalies

[22] In the next two figures, we examine the ULF response of the magnetosphere to isolated TIFP in greater detail. Figure 3 shows a shorter interval from 1630 to 1800 UT with two examples of the ULF response of the magnetosphere to isolated TIFP. The top four panels (left) are for the magnetic field magnitude, plasma flow speed, plasma number density, and dynamic pressure observed at THB (black) and THC (red) in the pristine solar wind and ion foreshock. There are several variations in all four parameters throughout the interval, which are more pronounced at THC and indicate the presence of TIFP (e.g., large reductions in the flow speed).

[23] The bottom four panels (left) are for data in the magnetosphere. The fifth panel shows an ion energy flux spectrogram for THEMIS-D (THD), which is located close to the magnetopause during this interval (see Figure 2, panels one and two). Enhancements in the energy flux of lower energy ions indicate crossings into the magnetosheath. The sixth and seventh panels in Figure 3 are for the electric and magnetic field perturbations observed at THEMIS-E (THE), which is located near noon, closer to the Earth than THD but outside geosynchronous orbit. The perturbation fields were computed by high-pass-filtering (frequency $> 1$ mHz) the data; these data were then rotated into a field-aligned coordinate system in which $z$ is along the background magnetic field, $y$ points eastward, and $x$ completes the right-hand orthogonal set (pointing radially outward at the equator). The eighth panel shows the magnetic field $z$ perturbations observed at geosynchronous orbit by G10 (blue), G11 (black), G12 (red), and THA (pink). Enhancements in wave activity seen in the bottom three panels are closely related to TIFP observed by THC.

[24] Two events of interest are marked by tan boxes at 1649 UT and 1724 UT. On the right of Figure 3, in inset 1, the same data as in the first to third panels and the eighth panel on the left of Figure 3 are shown for a shorter time interval. The total magnetic field at THC first decreases, then rapidly increases, and finally decreases to its original value. An increase in density is observed at the same time as the increase in the total magnetic field. Neither of these variations are observed further upstream at THB. These observations are consistent with the motion of the foreshock compressional boundary [*Omidi et al*., 2009]. Based on plasma observations (Figure 3, left, sixth panel)—in particular, the presence of higher energy ions prior to 1649 UT and absence after—and the position of the ion foreshock in the prenoon and dawn sector (Figure 2, panel 1), the foreshock compressional boundary was moving from dusk to dawn and THC exited the ion foreshock after passing through it. This motion would be expected to generate magnetic perturbations in the magnetosphere [*Russell et al*., 1997], and this is indeed the case as shown in the bottom panel of inset 1 (Figure 3, top right) and the bottom three panels of the main figure (left). Perturbations should be excited within a few minutes of the TIFP observation at THC, based on the expected transit times through the magnetosheath [*Samsonov*, 2011]. In this case, a transient perturbation is generated at THE's location, as seen, for example, in the magnetic field $z$ perturbation with a peak amplitude of about 6 nT. This perturbation is also seen at G10, G11, and G12 with a peak amplitude of about 2.5 nT.

[25] The time of the observation of peak amplitude is delayed from THC to G10 by 3 min, from G10 to G12 by about 30 s, and from G12 to G11 by about 2 min, as seen in the bottom panel of inset 1 (solid black triangles indicate the time when peak perturbation amplitude is observed to more clearly see time lags). G10 and G12 are separated by roughly [0.1,1.7] Re in GSM. Based on the 30 s time lag, this separation implies that a fast mode propagating purely in the GSM $x$ direction would be traveling at 21 km/s or purely in the $y$ direction at 361 km/s. Both of these estimates are unrealistically slow for typical fast mode propagation times, and thus the time lags cannot be due purely to fast mode propagation. However, these time lags could be consistent with the motion of the foreshock compressional boundary across the bow shock, in a dusk to dawn sense (based on the sequence of the peak amplitude observation) [*Sanny et al*., 2001]; the boundary may also move in a north-south sense, but that would not be effectively sensed at the GOES probes, which are at similar geomagnetic latitudes.

[26] The second event at 1724 UT is shown in inset two in the same manner as inset one. The top three panels indicate that the event is highly structured, because there are several rapid variations in the magnetic field and the density. These variations are most consistent with a pair of HFAs that formed around two IMF discontinuities observed by THC at ~17:24 and ~17:26 UT, respectively. They are associated with a large reduction in both the upstream flow speed and density (and thus the dynamic pressure) beginning at 1724 UT, which ought to excite ULF waves in the magnetosphere. This expectation is the same for an equivalent variation in the pristine solar wind [*Southwood and Kivelson*, 1990; *Eastwood et al*., 2011]. The bottom panel of inset two and the bottom four panels of the main figure (left) show that this transient event excites both ULF waves and magnetopause undulations. THD repeatedly crosses into the magnetosheath (fifth panel, left), unlike the event at 1649 UT. This is partly due to THD's outward motion, which has taken it closer to the magnetopause by 1724 UT; it is also due to the change in location of the ion foreshock region (compare panels one and two in Figure 2) and the different properties of this TIFP. THD's excursions into the magnetosheath appear to be quasi-periodic, suggestive of the excitation of a magnetopause surface mode. THE observes ULF wave perturbations in the electric and magnetic field with peak amplitudes of about 10 mV/m and 10 nT. G10, G11, and G12 see nearly simultaneous reductions and then increases in the total magnetic field, with amplitudes of 4 nT. This evidence suggests that, unlike the previous TIFP, this TIFP had a larger scale size and excited ULF waves globally.

### 3.4. Isolated TIFP Example: Foreshock Bubble

[27] Figure 4 shows another example of the ULF response to an isolated TIFP, in the same manner as Figure 3 (left). Two large reductions in the density, flow speed, and dynamic pressure are observed by THC at 2002 and 2005 UT, followed by rapid increases in the total magnetic field, density, and dynamic pressure. The observed sequence of increased density (2003 UT), reduced density (2004 UT), then increased density and strongly increased total magnetic field (2005 UT) is expected for the formation of a foreshock bubble and convection of the bubble downstream, where it ultimately impinges on the bow shock/magnetosphere [*Omidi et al*., 2010]. We could not determine the mechanism responsible for the first reduction in density at (2002 UT); it may represent the complexity of the FB structure or another FB entirely.

[28] The increased magnetic field, density, and dynamic pressure observed at THC at 2005 UT indicate the shock associated with the FB. Based on the shock normal direction ([0.98,0.21,0.01], GSM coordinates) and the location of the ion foreshock, the shock associated with the FB ought to impinge on the prenoon magnetosphere first and have the most significant impacts in that local time sector. This impact ought to affect the magnetosphere within a few minutes, although the expected time lag between the observation of the shock at THC and the impact in the magnetosphere is not as clear as the TIFP shown in Figure 3. One reason is THC's location near the edge of the ion foreshock (Figure 2, panel 4). Another reason is that typical models for the time lags for perturbations to traverse the magnetosheath after impinging on the bow shock are not necessarily applicable to FBs, which effectively reform the bow shock in the region upstream from the bubble [*Omidi et al*., 2010]. It is not clear how this process would affect the time delay between the observation of the shock at THC and the first observation of effects in the magnetosphere. Finally, the fact that the FB may be structured (e.g., there may be two FBs), based on the observation of two distinct density depletions at THC at 2002 and 2005 UT, may complicate the time lag analysis.

[29] With these caveats in mind, we now examine the response to the FB at the magnetopause and in the magnetosphere. As shown in Figure 4 (panel 5), THD crosses back and forth from the magnetosheath to the magnetosphere several times beginning at 2012 UT, indicating the presence of magnetopause undulations. This is consistent with the shock impinging first and most strongly on the magnetopause prenoon and then later closer to noon as the FB shock is convected with the solar wind flow. Magnetopause perturbations associated with the shock impingement would then arrive at THD's location in the postnoon sector at 2012 UT.

[30] We next examine the ULF response of the magnetosphere to the FB. Key times are indicated by black lines in Figure 4 to compare the ULF response at different probes. THE, located in the magnetosphere and very close to THD's position, observes a decrease in the $z$ component of the magnetic field at 2007 UT (indicated by first black line), followed by an increase in the same component at 2009 UT (second black line), then a decrease at 2012 UT (third black line), and finally an increase at 2015 UT (a little before the fourth black line) as shown in the seventh panel. We focus on the magnetic field $z$ component for the purpose of comparing with the probes at geosynchronous; however, we note that significant perturbations are observed in the other components with amplitudes of 10 nT in the magnetic field and 6 mV/m in the electric field. Panel eight shows that G11, located prenoon, sees an increase in the magnetic field $z$ component at 2009 UT (second black line), followed by a decrease at 2012 UT (third black line), and an increase at 2016 UT (fourth black line). G10/G12 do not see the magnetic field increase at 2009 UT, but they see the nearly the same signal as G11 after 2012 UT. C2, located near the dawn terminator and farthest from the magnetopause, sees a similar increase/decrease/increase sequence to G11, but delayed by approximately 2 to 3 min; however, this wave activity is not strongly increased above preexisting levels.

[31] The first decrease in the magnetic field observed at THE may have been related to the early stages of the formation of the FB. During this stage, a reduction in the $z$ component of the magnetic field would be expected as the magnetopause moves outward [*Omidi et al*., 2010]; this effect may be too weak to observe at the probes that are located farther from the magnetopause. The shock associated with the FB caused the magnetopause to move inward about 3–4 min after being observed at THC at 2005 UT and caused an increase in the $z$ component of the magnetic field at THE and G11 nearly simultaneously at 2009 UT. Beginning at 2012 UT, all probes in the dayside magnetosphere (THE, G10, G11, G12) observed the same increase

and decrease in the magnetic field $z$ component at nearly the same time (see seventh panel, $z$ component, and eighth panel—C2 also observed with a slight time lag). This may indicate that the FB excited a global mode [e.g., *Southwood and Kivelson*, 1990; *Hartinger et al*., 2012]. Alternatively, there may be additional TIFP subsequent to the FB, which directly drive these pulsations; THC would not observe these TIFP due to its location at the edge of the ion foreshock. The perturbations at GOES and THE terminate at approximately 2020 UT, but at least two wave cycles with Pc5 periods are observed by THE and G11 in conjunction with the FB. To our knowledge, this is the first report of ULF waves induced by a Foreshock Bubble.

### 3.5. Accumulated Response to Succession of TIFPs

[32] As shown in Figures 3 and 4, a variety of different TIFP can excite ULF wave activity. The properties of these waves vary depending on the properties of each TIFP and the foreshock morphology. However, the ULF waves share several similarities, including their global structure and Pc5 frequencies. These features are not unique to the short intervals shown in Figures 3 and 4; they are observed throughout the 8 h interval shown in Figure 1. However, during other periods, analysis of magnetospheric ULF wave activity is complicated by the fact that multiple TIFP affect the magnetosphere in rapid succession. For example, in a separate study analyzing this interval, Turner et al. (manuscript in preparation, 2012c) found that the repetition time between different TIFP between 2130 UT and 2300 UT is $\leq$5 min; this is far less than typical damping time scales for ULF waves, making it difficult to analyze isolated ULF wave events.

[33] Although we cannot examine the isolated ULF responses to a rapid succession of TIFP, we can say that the cumulative ULF response to these TIFP is similar to the response to isolated TIFP. As shown in Figures 1 and 2, the waves occurring during the period considered in this study have Pc5 frequencies and the location of the peak ULF response shifts in magnetic local time depending on the location of the ion foreshock; these characteristics are common to both waves associated with isolated TIFP (e.g., Figure 3) and waves associated with a succession of TIFP (e.g., Figure 1, 2130–2300 UT).

### 3.6. Differentiating Between Magnetospheric Pc3-4 Waves Driven by Upstream Waves and Pc5 Waves Driven by TIFP

[34] The ion foreshock is typically considered a source for magnetospheric ULF waves in the Pc3–4 frequency range (during low cone angle intervals) rather than the Pc5 frequency range. Magnetospheric Pc3–4 waves derive their energy from upstream ULF waves, whereas the Pc5 waves in this study derive their energy from TIFP pressure pulses; we would expect the properties of wave activity resulting from these two processes to be different. In order to examine the relative amplitudes and properties of Pc3–4 and Pc5 waves, we show an overview of ULF wave activity observed by G11 in Figure 5. The top panel is for the cone angle observed at THB after application of a 10 min smoothing window and the second panel is for the dynamic pressure observed at THC, which includes fluctuations caused by TIFP. The next four panels are for magnetic field fluctuations observed at G11. The perturbation magnetic field was computed by high-pass-filtering (frequency $>$ 1 mHz) the data, and these data were then rotated into field-aligned coordinates. The perturbation magnetic fields are shown in the third panel; Pc5 wave activity, particularly in the $z$ component, is correlated with dynamic pressure pulses observed at THC in the ion foreshock. During most periods, Pc5 waves have significantly larger amplitudes than Pc3–4 waves.

[35] The fourth through sixth panels are for the dynamic power spectra of the $x$, $y$, and $z$ magnetic perturbations. To better examine spectral features, we use the same technique as *Engebretson et al*. [1986], where the derivative of the time series is computed using a first difference technique and a fast Fourier transform (34 min) is applied. In the fifth panel (east-west magnetic perturbation), enhancements in power at discrete frequencies above 20 mHz (Pc3–4) indicate the presence of multiharmonic standing Alfvén waves (toroidal mode). They overlap in frequency and time with radial and compressional magnetic field perturbations with a more broadband frequency spectrum, as shown in the fourth and sixth panels. The enhancements in all components also overlap in time with periods of decreased cone angle (first panel) but can precede or occur after spikes in dynamic pressure corresponding to TIFP (second panel). Previous studies have established that multiharmonic standing Alfvén waves and compressional magnetic field perturbations in the dayside magnetosphere are connected [e.g., *Lessard et al*., 1999; *Clausen et al*., 2009]; they also showed that both occur during periods of low cone angle [e.g., *Chi et al*., 1994]. This connection suggests that ULF waves generated upstream in the ion foreshock are an important source of energy for the magnetospheric ULF waves with frequencies above the Pc5 range.

[36] The fourth and sixth panels also show Pc5 wave activity that is distinct from the wave activity with frequencies above 20 mHz (Pc3–4). These waves occur in bursts that are closely timed with dynamic pressure pulses observed at THC: they are associated with TIFP, unlike the higher frequency wave activity. Also, the Pc5 waves have mostly radial and compressional perturbations, whereas the higher frequency wave activity has both compressional and transverse perturbations. Different bursts of Pc5 wave activity have different polarizations in the $xz$ plane. For example, the Pc5 wave activity at 1649 UT induced by the foreshock compressional boundary has significant radial and compressional magnetic field perturbations (as indicated by the increased power spectral densities in the fourth and sixth panels, when compared to the fifth panel, in the 2–7 mHz frequency range). In contrast, the Pc5 waves at 1724 UT (hot flow anomalies) and 2005 UT (foreshock bubble) are associated with mainly compressional perturbations.

[37] Figure 5 shows that the ion foreshock is an energy source for both Pc5 and Pc3–4 waves during this period. TIFP drive Pc5 wave activity, whereas ion foreshock ULF waves drive Pc3–4 wave activity. The properties of the waves generated by each mechanism are very different: TIFP generate transient bursts of wave activity whereas upstream ULF waves generate steadier wave activity, and TIFP generate primarily compressional waves whereas

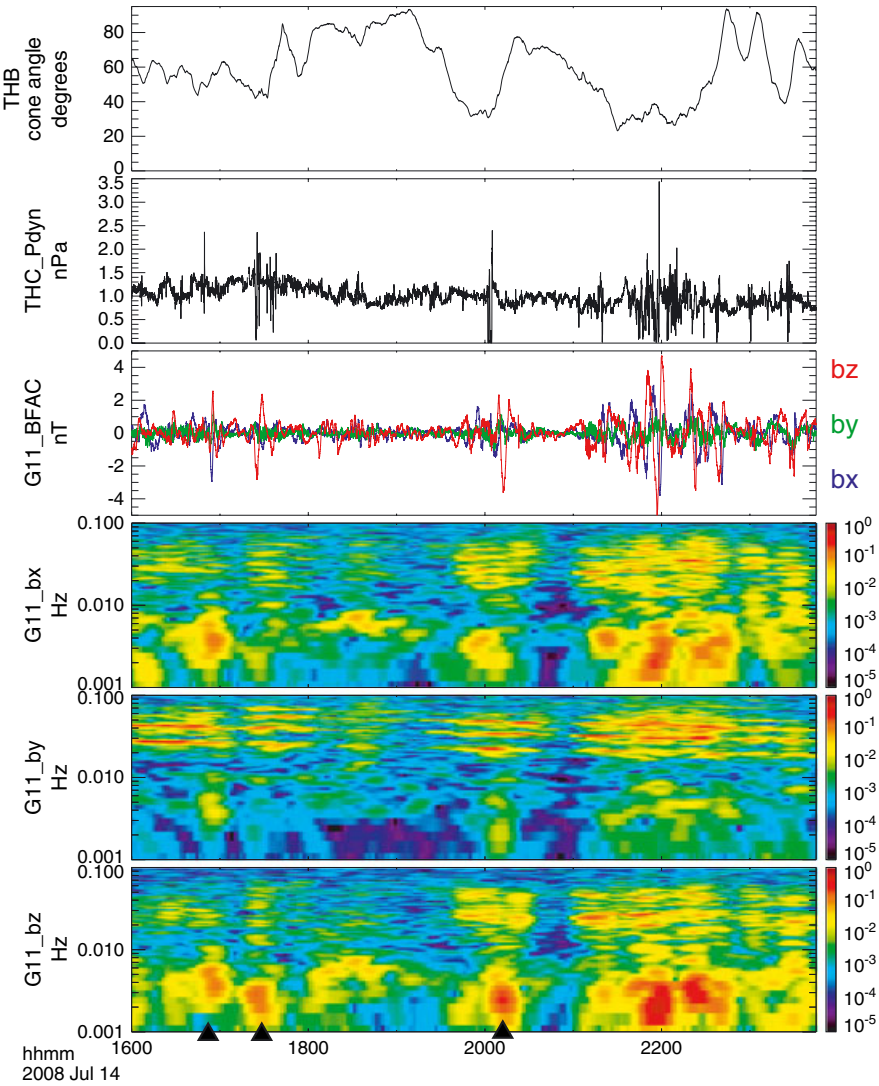


**Figure 5.** This plot shows an overview of ULF wave activity observed at geosynchronous orbit. Two classes of waves are observed, Pc3–4 perturbations (frequency $> 7$ mHz) with harmonic structuring and highest amplitudes in the east-west component and Pc5 (frequency $< 7$ mHz) perturbations strongest in the compressional and radial components. From top to bottom: (1) IMF cone angle observed at THB, (2) dynamic pressure observed at THC, (3) magnetic field perturbations observed at G11 in field-aligned coordinates, dynamic power spectra for the (4) radial, (5) east-west, and (6) field-aligned magnetic field perturbations.

upstream ULF waves generate both compressional and transverse magnetic perturbations.

## 4. Discussion

[38] In section 3, we showed spacecraft observations in the pristine solar wind, ion foreshock, at the magnetopause, and throughout the dayside magnetosphere on 14 July 2008 from 1600–2400 UT. During this period, there was little geomagnetic activity, no significant dynamic pressure pulses in the pristine solar wind, and higher than normal solar wind flow speed. The probes in the ion foreshock detected several pressure pulses corresponding to TIFP. These pulses generated ULF waves in the Pc5 frequency range in the magnetosphere with amplitudes comparable to storm time ULF waves (10 nT, 10 mV/m [*Walker et al.*, 1982]). The properties of these waves depended on the morphology of the ion foreshock; in particular, the local time sector with the largest amplitude wave activity was colocated with the ion foreshock. Wave properties also depended on the characteristics of the TIFP; for example, in some cases enhancements in wave activity were observed at different azimuthal locations with significant time lags, whereas in other cases they were observed simultaneously at all local times.

[39] The observed Pc5 waves are not driven by dayside reconnection: Pc5 waves generated by dayside reconnection are not typically observed at geosynchronous orbit [e.g., *Junginger and Baumjohann*, 1988; *Sanny et al.*, 2001], most Pc5 waves in this period do not have the traditional bipolar signature expected to be associated with transient

dayside reconnection [*Southwood et al*., 1988], and the Pc5 waves are associated with ion foreshock pressure pulses rather than IMF direction changes (several sharp IMF direction changes occur during the period without exciting Pc5 waves). These waves are also not driven by dynamic pressure fluctuations in the pristine solar wind: Pc5 waves occur after TIFP pressure pulses, which are an order of magnitude larger than pressure fluctuations in the pristine solar wind (~1 nPa compared to ~0.1–0.2 nPa). Finally, these waves are not driven internally: they have small azimuthal wave numbers in contrast to waves driven by drift-bounce resonance [*Southwood et al*., 1969], they do not occur during geomagnetically active periods in contrast to waves driven by drift-bounce resonance or the mirror instability [*Zhu and Kivelson*, 1991], and they have density and compressional magnetic perturbations in phase in contrast to the antiphase relationship expected for waves driven by drift-bounce resonance or the mirror instability (*Southwood et al*. [1969], *Hasegawa* [1969], *Zhu and Kivelson* [1991], based on data from THE, not shown in figures).

[40] There is substantial evidence in this event in favor of the driving of the Pc5 waves by TIFP:

[41] 1. Large pressure pulses resulting from TIFP observed in the ion foreshock directly precede enhancements in Pc5 ULF wave activity in the magnetosphere.

[42] 2. The ion foreshock pressure pulses are an order of magnitude larger than the pressure pulses in the pristine solar wind. These pressure pulses are comparable to those found in other studies (in the pristine solar wind) that resulted in significant ULF wave activity [*Eriksson et al*., 2006; *Sarris et al*., 2010].

[43] 3. The ion foreshock location determines the peak ULF response at geosynchronous.

[44] However, the KHI may also play a role in driving these Pc5 waves, particularly near the flank region where flow shear is larger. It is difficult to separate the effects of the KHI from the effects of TIFP in exciting ULF wave activity; it is possible that TIFP induce magnetopause disturbances, which grow to larger amplitude due to the KHI as they move tailward. However, based on the timing between the observation of the TIFP and the excitation of ULF waves, we conclude that TIFP is the essential component for exciting the Pc5 ULF waves in this study. Furthermore, although the high solar wind flow speed argues in favor of the KHI playing a role, the wide range of different IMF conditions for different periods of Pc5 wave enhancement argue against it; if the KHI were important, one would expect primarily northward or southward IMF to occur throughout the interval [*Chandrasekhar*, 1961; *Boller and Stolov*, 1973]. Instead, the IMF is often oriented in the GSM *xy* plane, which ought to lower the growth rate for surface waves; during some periods when the IMF is predominately northward, which ought to be the most favorable for the growth of surface waves due to the KHI, there is little or no wave activity in the magnetosphere (see Figure 1, 2110–2200 UT). Finally, we note that the observed fluctuations in dynamic pressure associated with TIFP were on the order of 1 nPa, comparable to the DC dynamic pressure and large enough to drive significant wave activity in the absence of a KH-unstable magnetopause [e.g., *Eriksson et al*., 2006; *Sarris et al*., 2010].

[45] The results in our study suggest that the ion foreshock plays a major role in generating ULF waves in the Pc5 frequency range in at least some cases. However, the ion foreshock is not considered a statistically important energy source for Pc5 waves because the correlation between Pc5 wave power and IMF cone angle is low when compared to the correlation with, for example, solar wind flow speed or pristine solar wind dynamic pressure [e.g., *Sanny et al*., 2007]. The comparison between the IMF cone angle and solar wind flow speed correlations is of particular interest, since the event in this study occurred during a high solar wind flow speed interval.

[46] Low cone angles indicate that the ion foreshock is colocated with the dayside magnetosphere, suggesting it will be more effective at driving ULF waves there, and indeed that is the case for Pc3–4 waves; typically, the IMF cone angle cutoff observed for upstream waves to drive Pc3–4 waves in the magnetosphere is $\theta < 45^\circ$ or $\theta > 135^\circ$. However, our results and several models of TIFP suggest that comparisons between ULF wave activity and the IMF cone angle may be more complicated for TIFP-induced Pc5 waves. Many TIFP, such as HFAs and FBs, occur in conjunction with IMF discontinuities, which would cause the IMF cone angle to rapidly change [e.g., *Omidi et al*., 2010]. Our results indicate that the degree of correlation with IMF cone angle depends sensitively on the interval chosen for the comparison; as shown in Figures 1 and 5, the IMF cone angle was not exceptionally low ($\theta < 45^\circ$ or $\theta > 135^\circ$) during or immediately following several isolated TIFP events in this study. The interval directly preceding the onset of ULF wave activity may be the best time to calculate the cone angle, before the passage of any IMF discontinuities associated with the TIFP. Furthermore, the IMF cone angle may not be a good indicator of the effectiveness of certain TIFP in driving Pc5 ULF waves; as shown in Figures 1 and 5, the cone angle is larger than 45° for much of the interval before 1930 UT, yet several TIFP drive significant Pc5 waves in the magnetosphere. Thus, TIFP may routinely drive Pc5 waves, despite the low correlations often found between IMF cone angle and Pc5 wave activity [e.g., *Chi et al*., 1994; *Sanny et al*., 2007].

[47] In many statistical studies, the correlation between Pc5 wave power and solar wind flow speed is significantly higher than the correlation between Pc5 wave power and IMF cone angle [e.g., *Sanny et al*., 2007]; this higher correlation is usually attributed to the increasingly KH-unstable magnetopause (and larger surface wave growth rates) at larger solar wind flow speeds [e.g., *Engebretson et al*., 1998]. We propose that this correlation may be at least partially explained by TIFP. Recent studies have shown that some TIFP are significantly more likely to be generated during high-speed solar wind intervals [*Sibeck et al*., 2001; *Facskó et al*., 2008, *Turner et al*., manuscript under review, 2012b]. Furthermore, TIFP can explain the dawn-dusk asymmetry often present in statistical studies of Pc5 wave activity, as previously noted by *Miura* [1992] and *Nosé et al*. [1995]. Finally, the TIFP events in this study, the supermagnetosonic jet event in the quasi-parallel magnetosheath described by *Hietala et al*. [2012] (note this magnetosheath jet was driven in a different manner than the jets described by *Archer et al*. [2012], which may not be correlated with solar wind flow speed), and four of six

events presented in the results of *Fairfield et al*. [1990] occurred during high-speed solar wind intervals ($V >$ 500 km/s); Pc5 waves were generated in all of these studies. Ground-based observations provide additional, suggestive evidence that high-speed solar wind intervals may be favorable for the excitation Pc5 perturbations via TIFP near the cusp and polar cap [*Kataoka et al*., 2003; *Murr and Hughes*, 2003]; these perturbations could be related to ULF waves in the magnetosphere [*Shields et al*., 2003].

[48] When placed in context with these previous studies, the results from this study suggest that TIFP may be an important energy source for Pc5 waves, perhaps as important as dynamic pressure fluctuations in the pristine solar wind, drift-bounce resonance, a KH-unstable magnetopause, or other more well established energy sources for Pc5 waves. In particular, correlations between IMF cone angle and Pc5 wave activity, previously used to argue against the ion foreshock as a source of Pc5 waves, may be misleading when specifically applied to Pc5 waves driven by TIFP. Additionally, correlations between solar wind flow speed and Pc5 wave activity, previously argued to be caused by the KHI, may instead be partially due to TIFP.

[49] One of the first studies to address the role of the ion foreshock in driving Pc5 waves was *Nosé et al*. [1995]; they conducted a study examining the relationship between Pc5 wave activity (with magnetic perturbations transverse to the background field) and the ion foreshock location for different solar wind flow speeds using 367 events. Our results, combined with recent models of specific TIFP, suggest that there are several reasons to revisit the results of *Nosé et al*. [1995] to more fully account for the role of TIFP in driving Pc5 waves:

[50] 1. *Nosé et al*. [1995] only examined transverse magnetic perturbations. Our results suggest the strongest Pc5 response to TIFP is compressional, at least near the magnetic equator.

[51] 2. *Nosé et al*. [1995] used a polar orbiting satellite and data coverage was not uniform at all magnetic latitudes. Compressional waves are attenuated at high latitudes, and thus are best observed near the magnetic equator [*Lee*, 1996]. If TIFP generate primarily compressional waves, the Pc5 response may be most clearly seen at the magnetic equator.

[52] 3. The data coverage in *Nosé et al*. [1995] was limited at the lowest and highest solar wind flow speeds [*Nosé et al*., 1995, Figure 5]. More data at these extremes may reveal the relationship between Pc5 wave activity and TIFP more clearly. Such data are available and have recently been used to study ULF wave power correlations with the solar wind [e.g., *Takahashi and Ukhorskiy*, 2007; *Liu et al*., 2010].

[53] 4. More well-established sources of Pc5 wave activity, such as compressional Alfvén waves driven by drift-bounce resonance, have been modeled extensively [e.g., *Southwood*, 1977] and examined in case studies [e.g., *Baumjohann et al*., 1987]. These studies revealed characteristics of the waves that could be used to identify them routinely in a statistical manner [e.g., *Hietala et al*., 2004]. Similar characteristics have not yet been identified for TIFP-driven Pc5 waves, and observations of TIFP-driven ULF waves suggest that there may be considerable variation between ULF waves resulting from different TIFP (e.g., this study showed mostly compressional wave activity whereas *Eastwood et al*. [2011] showed standing Alfvén waves). Until these characteristics can be identified, averaged values could be examined without concern for biases that arise due to the requirement that wave activity exceed a fixed threshold value, have a distinct spectral peak, have a certain polarization, etc. This suggests that a statistical examination of average power spectral density/amplitude rather than occurrence distributions, as examined by *Nosé et al*. [1995], may better show the effect of TIFP in driving Pc5 wave activity.

[54] 5. When IMF conditions are compared to magnetospheric wave activity, only averaged values of the IMF immediately preceding the onset of wave activity should be used (because of the rapid variation in the IMF that can occur in conjunction with TIFP).

[55] Based on the results of this study, *Nosé et al*. [1995] and other statistical studies of Pc5 wave power, other case studies showing the driving of Pc5 waves by TIFP, and the frequent occurrence of TIFP (particularly during high speed solar wind intervals), we argue that TIFP are an important source of Pc5 ULF waves in the Earth's magnetosphere. With the modifications listed above, a similar study to *Nosé et al*. [1995] could more fully quantify the role of TIFP in driving Pc5 wave activity.

## 5. Summary

[56] We presented observations of Pc5 ULF wave activity in the dayside magnetosphere during an interval of high-speed solar wind. These waves were driven by TIFP rather than dynamic pressure fluctuations in the pristine solar wind, dayside reconnection, or drift-bounce resonance with ring current ions. Although the period considered had little geomagnetic activity, wave amplitudes were as high as 10 nT and 10 mV/m, comparable to storm-time ULF wave activity [*Walker et al*., 1982]. Multispacecraft observations enabled continual monitoring of geosynchronous orbit (from dusk to dawn) and at three different locations upstream of the Earth's bow shock for a period of 8 h; this unique configuration enabled us to show the global ULF response of the magnetosphere to TIFP in periods with different ion foreshock configurations. At geosynchronous orbit, the probe in the local time sector closest to the ion foreshock observed the largest ULF response to the TIFP. Some TIFP-generated ULF waves were observed at different azimuthal locations with significant time lags, whereas others were observed simultaneously at all local times.

[57] Statistical studies of ULF wave amplitudes and recent theoretical and simulation work describing the properties of TIFP place these results in context: TIFP may be a primary energy source for Pc5 ULF waves in the magnetosphere, particularly during high-speed solar wind intervals. This study adds clarity to previous studies of Pc5 waves associated with the ion foreshock by specifically examining the role of TIFP. *Fairfield et al*. [1990] first showed that pressure pulses in the ion foreshock could drive Pc5 waves in the magnetosphere. Here we identify specific TIFP using recent models and show how the resulting ULF wave activity can vary significantly for different TIFP. *Nosé et al*. [1995] and *Sanny et al*. [2001] showed that peaks in Pc5 wave power were colocated with the expected location of the quasi-parallel bow shock in statistical studies; here, we use

a unique spacecraft configuration to directly show this relationship for the first time in a case study. Several studies have proposed that the ion foreshock functions primarily as a source of seed fluctuations for magnetopause surface waves, which grow due to the KHI [e.g., *Miura*, 1992]; here, direct measurements of dynamic pressure associated with TIFP enabled us to conclude that TIFP alone can drive large amplitude Pc5 waves, independent of a KH-unstable magnetopause. Several previous studies suggested that the ion foreshock was not an important energy source for Pc5 ULF waves on the basis of comparisons with IMF cone angle [e.g., *Chi et al*., 1994; *Sanny et al*., 2007]; here, we argue that these comparisons may be misleading when specifically applied to Pc5 waves driven by TIFP. Finally, we show how the results of this study can be used to design a new statistical study, motivated by *Nosé et al*. [1995], to quantitatively assess the role of the ion foreshock in driving Pc5 wave activity.

[58] **Acknowledgments**. We acknowledge NASA THEMIS contract NAS5-02099 and thank C. W. Carlson and J. P. McFadden for the use of the ESA data, D. Larson and R. P. Lin for the use of SST data, and K. H. Glassmeier, U. Auster, and W. Baumjohann for the use of FGM data provided under the lead of the Technical University of Braunschweig and with financial support through the German Ministry for Economy and Technology and the German Center for Aviation and Space (DLR) under contract 50 OC 0302. We acknowledge Elizabeth Lucek and the Cluster FGM team for use of the Cluster magnetic field data. We thank the NASA Space Science Data facility for use of solar wind data and geomagnetic activity indices. We thank David Sibeck and Robert McPherron for useful discussions.

## References

Angelopoulos, V., and D. G. Sibeck (2008), The THEMIS mission, *Space Sci. Rev.*, *141*, 5–34.

Archer, M. O., T. S. Horbury, and J. P. Eastwood (2012), Magnetosheath pressure pulses: generation downstream of the bow shock from solar wind discontinuities, *J. Geophys. Res.*, *117*, A05228.

Auster, H. U., et al. (2008), The THEMIS Fluxgate Magnetometer, *Space Sci. Rev.*, *141*, 235–264.

Balogh, A., et al. (2001), The Cluster Magnetic Field Investigation: overview of in-flight performance and initial results, *Ann. Geophys.*, *19*, 1207–1217.

Baumjohann, W., N. Sckopke, J. Labelle, B. Klecker, and H. Luehr (1987), Plasma and field observations of a compressional Pc 5 wave event, *J. Geophys. Res.*, *92*, 12,203–12,212.

Boller, B. R., and H. L. Stolov (1973), Explorer 18 study of the stability of the magnetopause using a Kelvin-Helmholtz instability criterion, *J. Geophys. Res.*, *78*, 8078.

Bonnell, J. W., F. S. Mozer, G. T. Delory, A. J. Hull, R. E. Ergun, C. M. Cully, V. Angelopoulos, and P. R. Harvey (2008), The Electric Field Instrument (EFI) for THEMIS, *Space Sci. Rev.*, *141*, 303–341.

Chandrasekhar, S. (1961), *Hydrodynamic and hydromagnetic stability*, Clarendon, Oxford.

Chi, P. J., C. T. Russell, and G. Le (1994), Pc 3 and Pc 4 activity during a long period of low interplanetary magnetic field cone angle as detected across the Institute of Geological Sciences array, *J. Geophys. Res.*, *99*, 11,127–11,140.

Chisham, G., and D. Orr (1997), A statistical study of the local time asymmetry of Pc 5 ULF wave characteristics observed at midlatitudes by SAMNET, *J. Geophys. Res.*, *102*, 24,339–24,350.

Clausen, L. B. N., T. K. Yeoman, R. C. Fear, R. Behlke, E. A. Lucek, and M. J. Engebretson (2009), First simultaneous measurements of waves generated at the bow shock in the solar wind, the magnetosphere and on the ground, *Ann. Geophys.*, *27*, 357–371.

Eastwood, J. P., E. A. Lucek, C. Mazelle, K. Meziane, Y. Narita, J. Pickett, and R. A. Treumann (2005), The Foreshock, *Space Sci. Rev.*, *118*, 41–94.

Eastwood, J. P., S. J. Schwartz, T. S. Horbury, C. M. Carr, K.-H. Glassmeier, I. Richter, C. Koenders, F. Plaschke, and J. A. Wild (2011), Transient Pc3 wave activity generated by a hot flow anomaly: Cluster, Rosetta, and ground-based observations, *J. Geophys. Res.*, *116*(A15), A08224.

Engebretson, M., K.-H. Glassmeier, M. Stellmacher, W. J. Hughes, and H. Lühr (1998), The dependence of high-latitude Pc5 wave power on solar wind velocity and on the phase of high-speed solar wind streams, *J. Geophys. Res.*, *103*, 26,271–26,384.

Engebretson, M. J., L. J. Zanetti, T. A. Potemra, and M. H. Acuna (1986), Harmonically structured ULF pulsations observed by the AMPTE CCE magnetic field experiment, *Geophys. Res. Lett.*, *13*, 905–908.

Eriksson, P. T. I., L. G. Blomberg, S. Schaefer, and K.-H. Glassmeier (2006), On the excitation of ULF waves by solar wind pressure enhancements, *Ann. Geophys.*, *24*, 3161–3172.

Facskó, G., K. Kecskeméty, G. Erdős, M. Tátrallyay, P. W. Daly, and I. Dandouras (2008), A statistical study of hot flow anomalies using Cluster data, *Adv. Space Res.*, *41*, 1286–1291.

Fairfield, D. H. (1971), Average and unusual locations for the earth's magnetopause and bow shock, *J. Geophys. Res.*, *76*, 6700–6716.

Fairfield, D. H., W. Baumjohann, G. Paschmann, H. Luehr, and D. G. Sibeck (1990), Upstream pressure variations associated with the bow shock and their effects on the magnetosphere, *J. Geophys. Res.*, *95*, 3773–3786.

Hapgood, M. A., M. Lockwood, G. A. Bowe, D. M. Willis, and Y. K. Tulunay (1991), Variability of the interplanetary medium at 1 a.u. over 24 years - 1963-1986, *Planet. Space Sci.*, *39*, 411–419.

Hartinger, M., V. Angelopoulos, M. B. Moldwin, Y. Nishimura, D. L. Turner, K.-H. Glassmeier, M. G. Kivelson, J. Matzka, and C. Stolle (2012), Observations of a Pc5 global (cavity/waveguide) mode outside the plasmasphere by THEMIS, *J. Geophys. Res.*, *117*(A16), A06202.

Hasegawa, A. (1969), Drift mirror instability of the magnetosphere, *Phys. Fluids*, *12*, 2642–2650.

Hietala, H., T. V. Laitinen, K. Andréeová, R. Vainio, A. Vaivads, M. Palmroth, T. I. Pulkkinen, H. E. J. Koskinen, E. A. Lucek, and H. Rème (2009), Supermagnetosonic Jets behind a Collisionless Quasiparallel Shock, *Phys. Rev. Lett.*, *103*(24), 245001.

Hietala, H., N. Partamies, T. V. Laitinen, L. B. N. Clausen, G. Facskó, A. Vaivads, H. E. J. Koskinen, I. Dandouras, H. Rème, and E. A. Lucek (2012), Supermagnetosonic subsolar magnetosheath jets and their effects: from the solar wind to the ionospheric convection, *Ann. Geophys.*, *30*, 33–48.

Hietala, M., R. Denton, M. Lessard, E. Miftakhova, and R. Anderson (2004), A study of Pc-5 ULF oscillations, *Ann. Geophys.*, *22*, 289–302.

Jacobs, J. A., Y. Kato, S. Matsushita, and V. A. Troitskaya (1964), Classification of Geomagnetic Micropulsations, *J. Geophys. Res.*, *69*, 180–181.

Junginger, H., and W. Baumjohann (1988), Dayside long-period magnetospheric pulsations - Solar wind dependence, *J. Geophys. Res.*, *93*, 877–883.

Kataoka, R., H. Fukunishi, and H. J. Lanzerotti (2003), Statistical identification of solar wind origins of magnetic impulse events, *J. Geophys. Res.*, *108*, 1436.

Lee, D.-H. (1996), Dynamics of MHD wave propagation in the low-latitude magnetosphere, *J. Geophys. Res.*, *101*, 15,371–15,386.

Lessard, M. R., M. K. Hudson, and H. Lühr (1999), A statistical study of Pc3-Pc5 magnetic pulsations observed by the AMPTE/Ion Release Module satellite, *J. Geophys. Res.*, *104*, 4523–4538.

Liu, W., T. E. Sarris, X. Li, R. Ergun, V. Angelopoulos, J. Bonnell, and K. H. Glassmeier (2010), Solar wind influence on Pc4 and Pc5 ULF wave activity in the inner magnetosphere, *J. Geophys. Res.*, *115*(A14), A12201.

McFadden, J. P., C. W. Carlson, D. Larson, M. Ludlam, R. Abiad, B. Elliott, P. Turin, M. Marckwordt, and V. Angelopoulos (2008), The THEMIS ESA Plasma Instrument and In-flight Calibration, *Space Sci. Rev.*, *141*, 277–302.

Miura, A. (1992), Kelvin-Helmholtz instability at the magnetospheric boundary - Dependence on the magnetosheath sonic Mach number, *J. Geophys. Res.*, *97*, 10,655.

Murr, D. L., and W. J. Hughes (2003), Solar wind drivers of Traveling Convection Vortices, *Geophys. Res. Lett.*, *30*, 1354.

Nosé, M., T. Iyemori, M. Sugiura, and J. A. Slavin (1995), A strong dawn/dusk asymmetry in Pc5 pulsation occurrence observed by the DE-1 satellite, *Geophys. Res. Lett.*, *22*, 2053–2056.

Omidi, N., and D. G. Sibeck (2007), Formation of hot flow anomalies and solitary shocks, *J. Geophys. Res.*, *112*, A08205.

Omidi, N., D. G. Sibeck, and X. Blanco-Cano (2009), Foreshock compressional boundary, *J. Geophys. Res.*, *114*(A13), A08205.

Omidi, N., J. P. Eastwood, and D. G. Sibeck (2010), Foreshock bubbles and their global magnetospheric impacts, *J. Geophys. Res.*, *115*, A06204, doi:10.1029/2009JA014828.

Paschmann, G., G. Haerendel, N. Sckopke, E. Moebius, and H. Luehr (1988), Three-dimensional plasma structures with anomalous flow directions near the earth's bow shock, *J. Geophys. Res.*, *93*, 11,279–11,294.

Russell, C. T., and M. M. Hoppe (1983), Upstream waves and particles / Tutorial Lecture/, *Space Sci. Rev.*, *34*, 155–172.

Russell, C. T., S. M. Petrinec, T. L. Zhang, P. Song, and H. Kawano (1997), The effect of foreshock on the motion of the dayside magnetopause, *Geophys. Res. Lett.*, *24*, 1439–1442.

Samsonov, A. A. (2011), Propagation of inclined interplanetary shock through the magnetosheath, *J. Atmos. Sol. Terr. Phys.*, *73*, 30–39.

Sanny, J., D. G. Sibeck, C. C. Venturini, and C. T. Russell (1996), A statistical study of transient events in the outer dayside magnetosphere, *J. Geophys. Res.*, *101*, 4939–4952.

Sanny, J., D. Berube, and D. G. Sibeck (2001), A statistical study of transient event motion at geosynchronous orbit, *J. Geophys. Res.*, *106*, 21,217–21,230.

Sanny, J., J. A. Tapia, D. G. Sibeck, and M. B. Moldwin (2002), Quiet time variability of the geosynchronous magnetic field and its response to the solar wind, *J. Geophys. Res.*, *107*, 1443.

Sanny, J., D. Judnick, M. B. Moldwin, D. Berube, and D. G. Sibeck (2007), Global profiles of compressional ultralow frequency wave power at geosynchronous orbit and their response to the solar wind, *J. Geophys. Res.*, *112*(A11), A05224.

Sarris, T. E., W. Liu, X. Li, K. Kabin, E. R. Talaat, R. Rankin, and V. Angelopoulos (2010), THEMIS observations of the spatial extent and pressure-pulse excitation of field line resonances, *Geophys. Res. Lett.*, *37*(A11), 15104.

Shields, D. W. et al. (2003), Multistation studies of the simultaneous occurrence rate of Pc 3 micropulsations and magnetic impulse events, *J. Geophys. Res.*, *108*(A6), 1225.

Shue, J.-H., J. K. Chao, H. C. Fu, C. T. Russell, P. Song, K. K. Khurana, and H. J. Singer (1997), A new functional form to study the solar wind control of the magnetopause size and shape, *J. Geophys. Res.*, *102*, 9497–9512.

Sibeck, D. G., R. B. Decker, D. G. Mitchell, A. J. Lazarus, R. P. Lepping, and A. Szabo (2001), Solar wind preconditioning in the flank foreshock: IMP 8 observations, *J. Geophys. Res.*, *106*, 21,675–21,688.

Sibeck, D. J., T. D. Phan, R. Lin, R. P. Lepping, and A. Szabo (2002), Wind observations of foreshock cavities: A case study, *J. Geophys. Res.*, *107*, 1271.

Sibeck, D. G., and V. Angelopoulos (2008), THEMIS Science Objectives and Mission Phases, *Space Sci. Rev.*, *141*, 35–59.

Singer, H., L. Matheson, R. Grubb, A. Newman, and D. Bouwer (1996), Monitoring space weather with the GOES magnetometers, in *Society of Photo-Optical Instrumentation Engineers (SPIE) Conference Series*, *Society of Photo-Optical Instrumentation Engineers (SPIE) Conference Series*, vol. 2812, edited by E. R. Washwell, pp. 299–308.

Southwood, D. J., and M. G. Kivelson (1990), The magnetohydrodynamic response of the magnetospheric cavity to changes in solar wind pressure, *J. Geophys. Res.*, *95*, 2301–2309.

Southwood, D. J., J. W. Dungey, and R. J. Etherington (1969), Bounce resonant interaction between pulsations and trapped particles, *Planet. Space Sci.*, *17*, 349.

Southwood, D. J. (1977), Localised compressional hydromagnetic waves in the magnetospheric ring current, *Planet. Space Sci.*, *25*, 549–554.

Southwood, D. J., C. J. Farrugia, and M. A. Saunders (1988), What are flux transfer events?, *Planet. Space Sci.*, *36*, 503–508.

Takahashi, K., and A. Y. Ukhorskiy (2007), Solar wind control of Pc5 pulsation power at geosynchronous orbit, *J. Geophys. Res.*, *112*(A11), A11205.

Thomas, V. A., and S. H. Brecht (1988), Evolution of diamagnetic cavities in the solar wind, *J. Geophys. Res.*, *93*, 11,341–11,353.

Troitskaya, V. A., T. A. Plyasova-Bakunina, and A. V. Gul'Elmi (1971), The connection of Pc2-4 pulsations with the interplanetary magnetic field., *Akademiia Nauk SSSR Doklady*, *197*, 1312–1314.

Turner, D. L., Y. Shprits, M. Hartinger, and V. Angelopoulos (2012a), Explaining sudden losses of outer radiation belt electrons during geomagnetic storms, *Nat. Phys.*, *8*, 208–212.

Turner, D. L.., N. Omidi, D. G. Sibeck, and V. Angelopoulos (2012b), First observations of foreshock bubbles upstream of Earth's bow shock: Characteristics and comparing to HFAs, *J. Geophys. Res.*, under review.

Turner, D. L., M. Hartinger, F. Plaschke, A. Kellerman, J. Wygand, V. Angelopoulos, and N. Omidi (2012c), The global impacts of transient ion foreshock phenomena on Earth's magnetosphere-ionosphere system, *J. Geophys. Res.*, in preparation.

Walker, A. D. M., R. A. Greenwald, A. Korth, and G. Kremser (1982), Stare and GEOS 2 observations of a storm time Pc 5 ULF pulsation, *J. Geophys. Res.*, *87*, 9135–9146.

Yumoto, K., T. Saito, and T. Sakurai (1983), Local time asymmetry in the characteristics of Pc5 magnetic pulsations, *Planet. Space Sci.*, *31*, 459–471.

Zhu, X., and M. G. Kivelson (1991), Compressional ULF waves in the outer magnetosphere. I - Statistical study, *J. Geophys. Res.*, *96*, 19,451.